AN IMPROVED HIBACHI SUPPORT STRUCTURE FOR ELECTRON-BEAM DIODE FOILS

Michael Kang, Bernard Weinstein, Evan Rose
Los Alamos National Laboratory
Los Alamos, NM 87545

Introduction

Large KrF amplifiers use electron beams to excite the laser gas. By necessity, the diode and laser cavity must be isolated by a mechanical barrier; an electron beam diode operates in vacuum, while the laser cavity may be filled with amagats of gas. Isolation is typically accomplished by a metal foil of low mass density which is mechanically supported by a structure having multiple open slots separated by ribs to permit passage of the electron beam. The support structure is referred to as a hibachi by reason of similarity.

Engineering design of a hibachi must take into consideration a number of issues. The foil material must have sufficient tensile strength to support the static and dynamic pressure load over each hibachi slot. The pressure load experienced by the entire foil is supported by the whole hibachi. Foil temperature rise (dependent on electron beam energy, current density, and foil properties) must not be excessive to the point where material strength is compromised. The design of the hibachi must minimize electron shading losses.

AURORA [1] is a KrF laser system at Los Alamos designed to demonstrate the feasibility of optical multiplexing for KrF lasers. The first two amplifiers in the amplifier chain are the Small Aperture Module (SAM) and the Pre-Amplifier (PA). This paper will describe the engineering design of replacement hibachis for the SAM and PA as part of a general upgrade to increase e-beam pumping. Hibachi shading loss mechanisms are briefly discussed. A simple model that calculates relative shading losses between hibachis for the axial field free case is presented. Based on modeling results, sample hibachi slots were fabricated and foils tested to destruction to verify standard membrane stress equation. Test results were used in the design and fabrication of hibachis that were installed on the amplifiers. Relative energy deposition measurements using capacitive manometers are presented.

The Small Aperture Module

The SAM is the first amplifier stage in the AURORA Amplifier System located between the twelve- and eight-fold encoding stations. It is directly driven by a 7-stage Marx generator with a peaking circuit and diverting switch set to provide a pulse of 200 ns FWHM. It operates at 350 kV and provides 46 kA at 70 kV charge. It is also frequently run at 65 kV charge for non-gain shots; its operating parameters are then 320 kV and 42 kA at the same pulselength. Its cold-cathode graphite felt emitter has dimensions of 101.6 cm X 11 cm. In its previous configuration, its hibachi also served as its anode. The previous hibachi consisted of a row of 53 vertical slots, each 13.65 cm high, 1.75 cm wide, and 2.54 cm deep, separated by ribs 0.16 cm wide as shown in Fig. 1. The hibachi material was Al 6061-T561. A 25 μm titanium foil was used.

An increase in the SAM hibachi transmission was attempted to increase the amplifier pumping intensity.

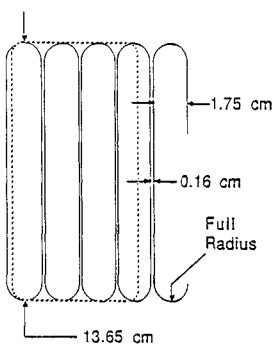

Figure 1. SAM slot configuration. Slot configuration prior to upgrade (solid); a slot of new design (dotted) is shown for comparison.

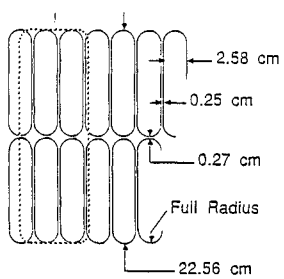

Figure 2. PA slot configuration. Slot configuration prior to upgrade (solid); a slot of new design (dotted) is shown for comparison.

The Pre-Amplifier

The PA, the second amplifier stage located immediately downstream of the 96-beam encoder, has a water dielectric Pulse Forming Line (PFL) of 2.7 Ohms and an output pulse length of 650 ns. The PFL is pulsed charged in less than 2 μs by a 14-stage Marx bank capable of 1.74 MV open circuit voltage.

The cold-cathode electron diode, with a graphite felt emitter of size 300 cm X 20 cm, routinely operates at 500 kV and 185 kA at 50 kV charge. An external axial guide field of 1200 G is used as the diode current exceeds the critical current for beam self-pinching.

The original diode had used a 300 cm X 40 cm emitter with a 20 cm high hibachi. The emitter had been made identical to the Intermediate Amplifier's (the next amplification stage) to reduce acquisition cost. As a result of the mismatch between PA emitter and hibachi, half the electron beam could not be used to pump the laser cavity. The PA's upgrade included the replacement of its cathode to recover the unused portion of the beam. The anode consisted of a 2.5 cm X 2.5 cm aperture wire grid; the entry face of the hibachi was located 2.54 cm downstream of the anode grid. The original hibachi, as shown in Fig. 2, consisted of three arrays of slots, each array of 66 slots separated from the next by a 4.83 cm X 2.54 cm rib required for mechanical strength. Each 33 X 2 array has vertical slots of size 11.14 cm high, 2.58 cm wide, and 2.54 cm deep, separated by ribs 0.25 cm wide. The hibachi material was Al 6061-T561. A 51 μm titanium foil was used.

The central rib that separates the rows of slots in the original PA hibachi caused a reduction in the pumping profile along the rib; this was shown by a small signal gain experiment to measure gain profile [2]. Single particle trajectories were also expected to worsen with the doubled current density. Based on these reasons, it was decided to replace the PA hibachi with one that alleviated these problems. The ultimate goal was a factor of 2 increase (via doubled current density) in pump power.

Electron Losses In the Foil Support Structure

A fraction S_g of the electron beam will be geometrically blocked by the hibachi structure. This is unavoidable as the tensile strength of available foils as of this writing do not permit single-slot hibachis of sizes on the scale of the diodes discussed above. This loss mechanism would be eliminated if such foils were available.

A fraction S_t, of the beam fraction $(1 - S_g)$ that enters the hibachi slots, will be lost within the structure due to skewed electron trajectories arising from the interaction between the propagating beam and its self-generated magnetic field. In the case of no applied axial magnetic field, such as SAM, this effect results in beam pinching. Critical currents at which beam pinch occurs for rectangular beams is calculated to be 95 kA for the SAM and 170 kA for the PA. Since the SAM's critical current is higher than its operating current, an external field is not absolutely required though the calculated beam footprint at the hibachi showed an area reduction of about 2. A guide field would be beneficial in preserving the beam footprint for uniformity. A pair of magnets was procured, but problems with its power supply, and the need to maintain global AURORA schedule, forced its temporary abandonment; it will be pursued when schedule permits. The discussion on SAM performance in this paper will be limited to the axial-field-free case only.

Simple Trajectory Model (Zero Axial Field Single Particle Orbits)

The equations of motion, with $B_z = 0$, in cartesian coordinates are:

$$\frac{d}{dt}(\gamma m v_x) = -q v_z B_y \qquad (1)$$

Report Documentation Page

Form Approved
OMB No. 0704-0188

1. REPORT DATE	2. REPORT TYPE	3. DATES COVERED
JUN 1989	**N/A**	**-**

4. TITLE AND SUBTITLE	5a. CONTRACT NUMBER
An Improved Hibachi Support Structure For Electron-Beam Diode Foils	5b. GRANT NUMBER
	5c. PROGRAM ELEMENT NUMBER
6. AUTHOR(S)	5d. PROJECT NUMBER
	5e. TASK NUMBER
	5f. WORK UNIT NUMBER
7. PERFORMING ORGANIZATION NAME(S) AND ADDRESS(ES) **Los Alamos National Laboratory Los Alamos, NM 87545**	8. PERFORMING ORGANIZATION REPORT NUMBER
9. SPONSORING/MONITORING AGENCY NAME(S) AND ADDRESS(ES)	10. SPONSOR/MONITOR'S ACRONYM(S)
	11. SPONSOR/MONITOR'S REPORT NUMBER(S)

12. DISTRIBUTION/AVAILABILITY STATEMENT
Approved for public release, distribution unlimited

13. SUPPLEMENTARY NOTES
See also ADM002371. 2013 IEEE Pulsed Power Conference, Digest of Technical Papers 1976-2013, and Abstracts of the 2013 IEEE International Conference on Plasma Science. Held in San Francisco, CA on 16-21 June 2013. U.S. Government or Federal Purpose Rights License.

14. ABSTRACT

15. SUBJECT TERMS

16. SECURITY CLASSIFICATION OF:			17. LIMITATION OF ABSTRACT	18. NUMBER OF PAGES	19a. NAME OF RESPONSIBLE PERSON
a. REPORT	b. ABSTRACT	c. THIS PAGE			
unclassified	**unclassified**	**unclassified**	**SAR**	**4**	

$$\frac{d}{dt}(\gamma m v_y) = q v_z B_x \quad (2)$$

$$\frac{d}{dt}(\gamma m v_z) = q v_x B_y - q v_y B_x + q E_z \quad (3)$$

where v_x, v_y, v_z are component velocities, B_x, B_y, and E_z are component fields, q and m are the electron charge and mass respectively, γ is the relativistic factor, and c is the speed of light. The displacement X , in the x direction, may be obtained from Eqns. 1 and 3 with the substitution:

$$\gamma = 1 + \frac{T(z)}{E_0} \quad (4)$$

where

$$E_0 = \text{abs}\left[\frac{\text{Electron rest energy}}{\text{Electron charge}}\right]$$

T(z) = electron voltage defined in Equation 7.

to obtain:

$$\frac{dX}{dz} = \frac{v_x}{v_z} = -\frac{B_y}{B_t}\frac{z}{\left[K(\gamma^2 - 1) - z^2\right]^{1/2}} \quad (5)$$

where $K = \left[\frac{mc}{qB_t}\right]^2$

$B_t^2 = B_x^2 + B_y^2$

and z is the displacement in the beam propagation direction. A similar equation is obtained for dY/dz.

$$\frac{dY}{dz} = \frac{B_x}{B_t}\frac{z}{\left[K(\gamma^2 - 1) - z^2\right]^{1/2}} \quad (6)$$

Equations 5 and 6 are solved for the normal displacements X and Y as a function of axial displacement z in two regions. The first region is the anode-cathode gap where the potential distribution for an infinite planar Child-Langmuir diode in the non-relativistic limit [3] T(z) is used in the expression for γ.

$$T(z) = V_0\left[\left(\frac{z}{d}\right)^{4/3} - 1\right] \quad (7)$$

V_0 = abs (cathode voltage)

d = anode-cathode spacing

The second region is the post-anode drift region where electron energy is a constant and no space-charge effects are included. The solution in the second region has an arbitrary constant that is determined by normalizing solutions at the anode. The field components B_x and B_y are calculated for a rectangular beam as described in [4].

For a rectangular emitter centered at z=0, y=0, and x=0, with the beam propagating in the z direction, and long dimension being the x direction, the solutions for Y and X are:

$$Y = +\frac{B_x}{B_t}\left[K(\gamma_0^2 - 1) - d^2\right]^{1/2} - \frac{B_x}{B_t}\left[K(\gamma_0^2 - 1) - z^2\right]^{1/2} + \frac{3dB_x}{2B_t}\left[\text{Term A}\right] \quad (8), \text{ and}$$

$$X = -\frac{B_y}{B_t}\left[K(\gamma_0^2 - 1) - d^2\right]^{1/2} + \frac{B_y}{B_t}\left[K(\gamma_0^2 - 1) - z^2\right]^{1/2} - \frac{3dB_y}{2B_t}\left[\text{Term A}\right] \quad (9)$$

where

$$\text{Term A} = \frac{(c' + b' + a')^{1/2} - (a')^{1/2}}{(c')} + \frac{1}{2(c')^{3/2}}\ln\left[\frac{2(c')^{1/2}(c' + b' + a')^{1/2} + 2(c') - 1}{2(a'c')^{1/2} - 1}\right]$$

$$c' = \frac{KV_0^2}{d^2 E_0} \qquad b' = -1$$

$$a' = \frac{2KV_0}{d^2 E_0}$$

$$\gamma_0 = 1 + \frac{V_0}{E_0}$$

A BASIC program was written to calculate geometric and trajectory shading losses of a hibachi having only vertical slots (as has the SAM) using equation (8) and (9). The program includes wall current corrections to the magnetic field by the method of images. This procedure does not describe the fields precisely since it assumes idealized return currents. Particle trajectories are calculated using the magnetic field at the point of emission over the full trajectory and corrections to the electric potential are not made based on beam pinching. The equations are not time-dependent; single-value cathode voltage and current density are assumed. However, this simple approach appears to predict relative transmissions that agree with measured results.

The intent of this exercise was to provide the hibachi designer with a useful tool to provide a relative figure of merit for various hibachis under consideration. At present this program will only work for hibachis with one row of slots, i.e., only vertical ribs.

The calculation of losses are done in the following manner: the emitter is divided up into an array of emitting sites, and the projected beam area on the hibachi ribs is obtained by calculating X and Y normal displacements for emitter edge electrons and calculating the area within the envelop of these electrons. The overlap area between the beam footprint at the hibachi and hibachi ribs themselves is then known since the rib locations are part of user input. This overlap area constitute the geometric loss area. The beam, reduced by the rib-intercepted portion, now becomes the new beam area to be used in calculating trajectory shading loss, i.e., electrons lost to the sides of ribs. The trajectory-shaded distance due to each rib is the difference in the X displacements between hibachi entry and exit planes for vertical ribs; the shaded area is the product of the shaded distance and rib height. The lost fraction is the beam area which overlaps hibachi structures divided by the total beam area.

Some conclusions from numerical calculation:

1. Thin hibachis with the largest possible slots have the least shading. Ever-diminishing returns on transmission is obtained as hibachi thickness is progressively reduced (shallow hibachi ribs) or slot area progressively increased (few hibachi ribs).

2. The vertical displacement of edge electrons along the long emitter dimension, calculated at the foil plane, is largest for those electrons at the central portion of the long edge. The horizontal displacement

shows a similar trend along the short dimension. Hence the simple model predicts the e-beam footprint on the foil is slightly bone-shaped.

3. The model demonstrates that the optimal slot configuration for a rectangular diode without external field is obtained by orienting the slots with their long sides normal to the local magnetic field. For a long skinny cathode, this translates into a single row of vertically-oriented slots (perpendicular to the long emitter dimension).

Equations that describe other aspects of the same problem may be found in [5], [6], and [7] for the interested reader.

Mechanical Design

Aluminum 2024-T81 was chosen as the foil material in the SAM for its relatively high tensile strength (for an aluminum alloy), its resistance to fluorine attack, and its low atomic number; the small laser aperture size made reflectivity a non-issue. Its thickness of 61 μm was inadvertently chosen from its availability. The calculated temperature rise for this material was estimated to be approximately 80 C using measured SAM voltage and current waveforms measured at the bushing; the bushing inductance was not taken into account in this estimate of voltage. This temperature rise was considered to be safe for Al 2024-T81 since its strength does not substantially decrease until 150 C to 200 C is reached. The calculated temperature rise was estimated to be approximately 90 C for 61 μm Al foil and 120 C for 51 μm Ti foil for the PA. The back-up position, should aluminum foils fail due to beam hotspots, would be to revert to titanium foils.

Past experience with membrane stress equations had indicated that these equations were too conservative for the design of hibachi slot sizes. These equations applied to design of the Intermediate Amplifier hibachi resulted in a structure whose foil failed to rupture at pressures greater than 150% of the designed point. This experience, together with reduced stress at the rib edge (from elliptical profiling of the rib edges [8]), led to a short testing program to measure burst pressures of specific slot sizes of interest. Tensile stress at the center of the foil, calculated from burst pressure data, can then be compared with the ultimate tensile stress of 65,000 psi quoted by the vendor.

The test fixture is shown in Fig. 3. The slot edge design incorporates the Avco Everett Research Laboratory recommendation, and all surfaces in contact with the foil were polished to a 16 μ-inch finish. The differential pressure across the foil was repeatedly cycled from zero to a preset level by a timer-operated solenoid valve to simulate the mechanical service the foil would undergo. Each cycle consisted of applying pressure to the foil, holding it for about a minute, and venting. Pressure could also be introduced and released manually by a bypass toggle valve. While this procedure did not simulate the dynamic pressure loading due to energy deposition in the laser gas, it was felt that this was a cost effective compromise with reality, given that a safety factor would be incorporated into the final slot design.

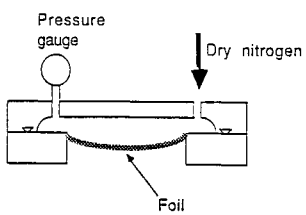

Figure 3. Foil pressure test fixture. A timer-operated solenoid valve (not shown) fills and vents the test fixture once a minute.

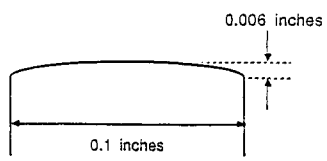

Figure 4. Hibachi rib. Cross-section of hibachi rib showing 8:1 ellipse profile.

Ten foils were tested in two different slot configurations shown in Table 1. The number of samples was small; limited manpower was available at the time to perform these tests, and testing was stopped altogether when data was deemed sufficient to extract a tensile strength with high confidence. Foils shown in the table as surviving 1 cycle were intentionally ruptured to obtain an upper limit on preset pressure. Foil 5 failed after 1918 cycles at a lower pressure; we hazarded the guess that this was due to some defect local to this sample since foil 6 exceeded foil 5 in cycle number and burst pressure. Foils 6 and 10 did not rupture by themselves at all. Foil 6 survived 1815 cycles at 32 psig, had its pressure increased to 36 psig for another 888 cycles, and failed at 47 psig when pressure was manually increased. Foil 10 survived 1255 cycles at 32.5 psig, and ruptured when pressure was manually increased to 34 psig. The data shows large scatter, perhaps from individuality of specific areas of foil, or failure to maintain consistent edge clamping conditions. However, the results showed that foils easily survived repeated cycling in the thousand shot range at 90% of the lowest single-shot rupture pressure for each slot size. The stress S in the center of the foil is given by [9]

$$S = n_2 \left[\frac{p^2 l^2 M}{t^2} \right]^{1/3} \qquad (10)$$

where S = stress in the center of the foil (psi)
n_2 = dimensionless coefficient from Fig. 7.5, Ref [9]
p = static plus twice expected dynamic pressure (psi)
l = length of slot (inches)
E = modulus of elasticity of foil material (psi)
t = foil thickness (inches)

This equation is the most reliable one to use as the location of interest is far removed from the edge stress induced by local clamping conditions [10]. Using the lowest single-shot rupture pressure for each slot size in the above equation, tensile stresses of 133,000 psi and 141,000 psi are calculated for the 3.175 inch wide, and 4.167 inch wide, slots respectively. These numbers are in close agreement with each other but differ vastly from the vendor rated and tested value of 65,000 psi. A safety factor of 1.5 was applied to the lower of the two numbers; this gives a value of 88,600 psi to be used in design. The design parameters used, and the resultant hibachi slot sizes for the SAM, are given in Table 2. The SAM hibachis consists of a row of vertical slots separated by vertical ribs 0.254 cm wide. The slot edges have elliptical profiles as shown on Fig. 4. Hibachi depth is calculated by requiring individual ribs to support the loading on half of each adjacent slot. Hibachi depth is minimized by using high strength materials; aluminum 7075-T651 was chosen for its easy machinability and strength.

TABLE 1

Foil#	Slot opening in. X in.	preset pressure psig	#cycles	fracture pressure psig	calculated stress at center, psi
1	8.880 x 3.175		1	44	150,660
2	8.880 x 3.175		1	41	143,700
3	8.880 x 3.175		1	43	148,300
4	8.880 x 3.175		1	40	141,400
5	8.880 x 3.175	30	1918	30	116,700
6	8.880 x 3.175	32	1815		
		36	888		
			1	47	157,400
7	8.880 x 4.167		1	37	140,600
8	8.880 x 4,167		1	36	138,100
9	8.880 x 4.167		1	36	138,100
10	8.880 x 4.167	32.5	1255		
			1	34	132,900

Test data for the 10 foils tested. Calculated stress uses equation 10 with p = fracture pressure (psig), M = 10.6e6 psi for aluminum, n_2 = 0.23 for the 3.17 inch wide slot, and n_2 = 0.241 for the 4.176 inch wide slot.

TABLE 2

	SAM	PA
Static pressure (Torr)	1200	900
Dynamic pressure (Torr)	125	340
Inferred ultimate stress (psi)	132,900 (test foil 10)	141,400 (test foil 4)
Safety factor	1.5	1.375
Foil working stress (psi)	88,600	102,800
n_2	0.255	0.200
Slot length (inches/cm)	5.375/13.65	8.880/22.56
Slot width (inches/cm)	2.737/6.95	2.970/7.54
Rib width (inches/cm)	0.1/0.25	0.1/0.25
Corner radius (inches/cm)	0.25/0.64	0.5/1.27
Rib depth (inches/cm)	0.5/1.27	0.875/2.22

Design parameters and final slot sizes for the SAM and PA. Oth parameters used are t = 0.0024 inches and M = 10.6e6 psi for aluminum.

Design parameters for the PA hibachi slots are also shown in Table 2. When the PA hibachi was designed some time after the SAM's, the safety margin used in design was decreased in two ways. We had noted that the narrower slots of the test fixture, whose physical dimensions were close to the probable final design dimensions for the PA hibachi slots, had a minimum burst pressure of 40 psig (foil 5 datapoint was ignored for reasons mentioned earlier); this translates to a stress of 141,400 psi at foil center. A lowered safety factor of 1.375 gives a working stress of 102,800 psi. It was felt that these choices would be adequate since these were based on actual burst data.

Both the SAM and PA have hibachis built into their diode boxes. The existing hibachi ribs in both amplifiers were completely machined away and new hibachis fabricated to seal over the opened apertures. This retrofit method increased the post-anode drift regions in the SAM by 1.27 cm, and in the PA by 2.22 cm. In addition, a new anode was fitted to the SAM. This consists of a row of 254 m wires spaced 0.635 cm apart; its geometric transmission is 0.96.

Table 3 shows the calculated relative transmissions for the SAM. The calculated relative increased transmission of the new SAM hibachi, and hence the expected increase in energy deposition, is 22 %.

TABLE 3

	SAM before upgrade	SAM after upgrade	Relative change
Geometric Transmission ($1 - S_g$)	0.917	#0.930	1.014
Trajectory Transmission ($1 - S_t$)	0.810	0.970	1.198
	Net relative change		*1.215*

Calculated relative hibachi transmission for the SAM. # includes geometric transmission of 0.96 for anode grid.

SAM Experimental Results

When the new hibachi and aluminum foil were installed, hotspots in the beam occasionally punctured the foil at random locations. As reliability was of high importance, aluminum foil was abandoned in favor of Ti foil which has a much higher melting temperature. A 38 μm Ti foil was used.

A Barytron model 2220A-01000AB-SP094-82 capacitance manometer mounted on the SAM laser cavity had previously measured a 55 Torr pressure rise with 900 Torr of 0.5% F_2, 10% Kr, and 89.5% Ar mix at diode parameters of 350 kV, 46 kA, and 200 ns FWHM prior to the hibachi change. This measurement had been performed with a 25 μm Ti foil.

The pressure jump measurement was repeated with the new hibachi under the same pulsed power and gas conditions. Energy deposition increased from 585 J to 800 J, an increase of 35 % (versus 22% predicted by the model). We feel the discrepancy between calculated and measured values is largely due to simplifications made in calculating the magnetic field. A higher field (as would be true for a converging beam) would result in a higher trajectory shading loss for the old hibachi and hence make the relative increase higher; the new hibachi is so transparent that increased fields probably would not significantly increase its shading losses.

PA Experimental Results

Aluminum foil worked well mechanically in this design though plagued with failures from beam hotspots. A 38 μm Ti was substituted instead. The frequency of failures dropped but did not stop altogether. Evidence of damage from aluminum-anode return currents at the failure sites were observed on the cathode. The failures occurred closer to hibachi ribs than the center of slots. On the last failure, melted blobs of aluminum (from the hibachi) that landed on the foil were found; they were surrounded by heavy discoloration of the Ti foil (indicating heating). We surmised that the current density (34 A/cm^2) was high enough to cause vaporization of the hibachi material. While this by itself did not cause foil failures directly, the odd blobs of molten material that landed on the foil either weakened it, or caused an extraordinary amount of beam energy to be stopped at these sites on subsequent shots. The problem went away after the upstream side of the hibachi was covered with Ta and W foil.

A pressure rise of 168 Torr had previously been measured with 750 Torr of 0.5% F_2, 10% Kr, and 89.5% Ar mix at Marx bank charge of +/- 55 kV (cathode voltage 550 kV). This corresponds to 9.9 kJ deposited energy. Owing to jitter problems with the Marx generator and output switch during the assigned checkout period, it was not possible to measure laser cavity energy deposition at the same pulsed power levels for direct comparison to the model.

At present, pressure rise is routinely 300 Torr at +/- 50 kV Marx generator charge (cathode voltage 500 kV), corresponding to 17.7 kJ deposited energy into a laser mix of 0.3% F_2, 10% Kr, and 89.7% Ar. This is a conservative number as deposited energies as high as 18.9 kJ have been measured at the same pulsed power levels (depending on PFL switchout time). Applying $V^{1.5}$ scaling to the deposited energy for a 1 sided pump, 345 Torr or 20.4 kJ deposited energy can be expected at +/- 55 kV Marx bank charge. This translates to a relative increase of 2.05 (ratio of 345 to 168 Torr). Hence the new hibachi appears to have met the design goal of doubled pump power.

Summary

An ultimate tensile strength of almost twice the published value for aluminum 2024-T81 was inferred from foil burst tests. The inferred value was used in designing slot sizes for hibachis that were fielded in the SAM and PA in AURORA. An expected relative gain in hibachi transmission of 1.22 was calculated for the SAM hibachi using a simple single-particle orbit model; this was in fair agreement with experimental measurement of 1.35 . An increase of 1.8 in PA energy deposition was measured at +/- 50 kV Marx generator charge. $V^{1.5}$ scaling indicates that energy deposition should be twice that measured prior to the upgrade at +/- 55 kV charge.

Acknowledgements

The authors wishes to thank Byron McLoud, Roger Shurter, Dana Netz, and the AURORA Operations crew for their contributions to this effort.

References

[1] L. A. Rosocha, P. S. Bowling, M. D. Burrows, M. Kang, J. Hanlon, J. McLeod, and G.W. York, Jr., "An Overview of AURORA: A Multi-KiloJoule KrF Laser System for Inertial Confinement Fusion," Lasers and Particle Beams, Vol. 4, pp. 55-70, 1986

[2] D. P. Greene, Los Alamos National Laboratory, Unpublished work.

[3] C. L. Hemenway, R. W. Henry, and M. Caultron, Physical Electronics, pp. 108, John Wiley & Sons, 1962.

[4] J. H. Jacob, M. J. W. Boness, and J. C. Hsia et al, "Visible (XeF) Laser Scale-Up," Avco Everett Research Laboratory, Inc., Final Report on DARPA Order No.35809, Dec. 1982.

[5] L. A. Rosocha, and K. B. Riepe, "Electron-Beam Sources For Pumping Large Aperture KrF Lasers," Fusion Technology, Vol. 2, pp 576-611, May 1987

[6] L. G. Schlitt, and L. P. Bradley, "The Physics Of Relativistic Electron Beams In Rectangular And Cylindrical Geometries," SAND76-5122, pp. 239-251, Sandia National Laboratories, Nov. 1975.

[7] S. Putnam, "Theoretical Studies Of Intense Relativistic Electron Beam-Plasma Interactions," PIFR-72-105, Physics International Company, July 1972.

[8] M. W. McGeoch, A. J. DeFuria, and C. T. Pike, "Pulsed Electric Discharge Laser Technology - Electron Beam Window Foil Material," Avco Everett Research Laboratory, Inc., Final Report on DARPA contract DAAH01-82-D-A013, Jan 1984.

[9] E. E. Sechler, and L. G. Dunn, "Airplane Structural Analysis and Design," pp. 288, Dover Publications, Inc., 1963.

[10] E. Yarvornik, Los Alamos National Laboratory Memo L-10/TM/77-171, Dec 1977.